Body Surface Cardiac Propagation Maps of Humans from Laplacian Moments of Activation

W.G. Besio, C.C. Lu, P.P. Tarjan

Department of Biomedical Engineering, College of Engineering

University of Miami, Coral Gables, FL

Abstract—In this feasibility study Laplacian electrocardiograms were utilized to generate body surface moment of activation (MOA) maps. The data were obtained with Laplacian sensors from humans. Inverse distance interpolation was applied to improve the image quality. For normal subjects, the MOA maps showed certain common features. A partial activation cycle of atrial flutter was mapped and is presented. Further studies must be conducted to determine the diagnostic potential of such patterns based on a larger number of subjects.

1 Introduction

The cardiac activation spread is a spatial and temporal function that can be detected on the body surface. The typical 12-lead ECG provides useful global temporal assessment of the propagation in the ventricles, but it yields limited spatial information. Some arrhythmias cannot be localized using the standard 12-lead ECG and further diagnostic techniques are necessary, such as an invasive electrophysiology (EP) study. Non-invasively obtained spatial information about cardiac activity, derived from body surface potentials, may be important in reducing the time for invasive EP exploration. A non-invasive system with both, high spatial and temporal resolution, may be useful to determine the origin of an arrhythmia.

Improved spatial resolution beyond the 12-lead ECG was obtained in the past with multi-lead ECG body surface potential mapping (BSPM). Extensive studies of these BSPMs have been conducted since the 1950s concerning the source of the electrical

1

activity and its propagation [1-6]. These sequential, instant-by-instant BSPMs reflect the depolarization spreading through the heart. Body surface equipotential contours give a snapshot of the depolarization state. Isochronal maps depict those contours, which are depolarized at the same instant.

Fattorusso and Tilmant [7] appear to be the first investigators who observed cardiac signals from the body surface utilizing a concentric bipolar sensor that displayed more localized information than unipolar precordial leads. Van Oosterom and Strackee [8] reported that a concentric bipolar sensor, placed on the surface of the conducting medium, does emphasize the contributions of electric sources lying directly underneath the body surface, compared with the contributions of more distant sources. The concentric bipolar electrode emphasizes the activity between its inner disc and the inner radius of its annulus.   Reducing this gap accentuates local sensitivity, however it also reduces the sensitivity with depth. The concentric sensor is rather insensitive to signals arising beyond its outer annulus. Kaufer's [9] thesis supported Van Oostrom's findings.

Surface Laplacian ECG (LECG) was another advance in non-invasive imaging. According to Geselowitz and Ferrara [10], Laplacian sensing of surface potentials was first proposed by Hjorth [11] for studying the electroencephalogram (EEG), and later by He and Cohen [12] for electrocardiography (ECG).

He and Cohen [13] reported that a special bipolar 'Laplacian' surface sensor produced higher resolution maps than BSPMs. Wu et al. [14-15] have been estimating LECG from potential measurements using an array of disc electrodes. Their work suggests that it is feasible to estimate the body surface Laplacian maps (BSLMs) from potentials using a finite difference algorithm over the anterior chest in male subjects. They reported higher spatial resolution with their algorithm than with BSPM. He [16] suggested that, in theory, it might be possible for the Laplacian ECG to provide implicit spatial information regarding moving wavefronts within the myocardium, which is

contained, but below clear detection, in the body-surface-potential distribution. Our work is exploring this concept. To further advance this technology, our target is to develop a non-invasive multimodal system that shows cinematic images of the dynamically changing surface of the heart along with the electrical activity projected on that surface in real time. Towards this goal, active sensors were developed by Lu, Tarjan et al. [17-20]. Each sensor consists of three concentric elements; the central disc, as depicted in Fig. 1, is shorted to the outer ring and serve as an electrode vs. the inner ring. The output of these sensors may be described by equations 1.

Figure 1 about here

$$V_{tot} \cong \frac{1}{2}(V_o + V_c) - V_m = \frac{1}{2}[(V_o - V_m) + (V_c - V_m)] = \frac{1}{2}(\Delta V_{om} - \Delta V_{mc}) \approx \frac{\partial^2 V_{sfc}}{\partial s^2} \qquad \text{Eq. 1}$$

where V_o, V_m and V_c refer to the potentials of the outer, middle and central elements and s is radial in any direction. The signal to noise ratio (SNR) was improved by mounting the signal processing electronics directly on the "active" sensor.

The data for our analysis was acquired by Lu and Tarjan, along with two cardiologists, Antonioli and Argnani, from cardiac patients in Ferrara, Italy, in 1997 and 1998. The active sensors and the data acquisition system were presented in Lu's dissertation [20]. The active sensor for data acquisition had a pass band from 5 to 500 Hz with a gain of 1000. The signal was digitized at 1000 Hz to achieve 1 ms resolution over 30 second episodes, or 30,000 samples per channel for each episode.

2 Methods

For this feasibility study, the records of twenty-six subjects were evaluated: six normals (age 20-37 y.) and twenty with various pathologies (29-85 y.). Three subjects with atrial flutter were studied, one of those, AS, is presented here. For subject AS, 7 LECG channels and the Lead II ECG (L2) were recorded simultaneously and repeated

several times with the sensors moved to various locations on the chest. The normals were recorded with only two concurrent channels: LECG and L2. The digital signal processing programs were written using Matlab 5.3 by MathWorks. The raw data was windowed at 800 points, 800 ms, 400 before and 399 after the peak of the L2 QRS (L2R), filtered and averaged. These sensors are characterized by their high spatial resolution along with strong far-field rejection. In addition, the active sensors improve the SNR. Despite these advantages, additional filtering was necessary. One of our signal detection techniques, to determine the moment of activation (MOA), is based on zero crossing; therefore low noise on the baseline is critical. A Wiener filter, similar to that of Bertrand et al. [21], a sub-average spectral analysis adaptive Wiener Class III filter was utilized to filter each window. This filter is implemented using the average of the spectra of all the windows and the spectrum of the time averaged windows. These filtered windows, or fixed length segments of individual heart cycles, are then signal averaged to enhance the SNR.

As the distance increases between the electrically active tissue and the sensor on the surface of the chest, the task to detect the MOA becomes progressively more difficult. The MOA is defined for our purposes as the instant the dipole that represents the depolarization wavefront crosses the vector normal to the active sensor's surface. We tested four MOA detection techniques on our data from human subjects:

(1) the simple delay from the L2R to the LECG peak (MOA1);

(2) cross-correlation of the L2 and LECG (MOA2);

(3) cross correlation of the L2 ECG derivative and the LECG (MOA3); and

(4) the delay from the L2R to the steepest zero crossing of the LECG (MOA4).

For the cross-correlations, the absolute maximal value was found and the time shift from the L2R was defined as the MOA (MOA2 and MOA3). These four techniques did not always yield closely grouped values for the same event.

A study of MOAs from the 3-point moving average of single beats, instead of the resulting signal from signal averaging the filtered windows, was conducted on the data from the six normal subjects to compare the four detection techniques. The coefficient of variance (CV), the ratio of the standard deviation to the mean, of the single beat MOAs was employed as a figure of merit. No single technique emerged as the most desirable one. Under various circumstances different techniques appeared to be better than others.

We established rules for selecting the most appropriate MOA among the four methods depending on the quality of the LECG data. If the derivative cross correlation (DCC) coefficient leading to MOA3 was greater than 0.7, then it usually had the smallest CV among the four methods, and MOA3 was used regardless of the others. If the DCC was less than 0.7 and the "regular" cross correlation coefficient (RCC) was greater than 0.8, then MOA2 would be used for the map. If neither the DCC, nor the RCC was acceptable, and the SNR was greater than five, without multiple zero crossings of the signal, then the zero crossing technique (MOA4) was applied. It was evident that whenever the SNR was above 20, all four techniques yielded small CVs. The resulting process for MOA determination, following the single beat analysis, is outlined in Fig. 2. The "demean" routine prior to the MOA determination removes the DC offset. Isochronal body surface MOA maps (BSMOAMs) were then generated using the MOA values.

Figure 2 about here

For subject AS, a 79-year old male with atrial flutter and impaired AV conduction, a different method was used for signal processing than described above for the atrial flutter maps. A 3-point moving average was used to smooth the raw data. Since the atrial flutter was perceptible in L2, a threshold was set to synchronize the LECG channel windows to the L2 atrial flutter. To improve the SNR, these windows were synchronized and signal averaged with respect to the peaks corresponding to the flutter waves in L2 (L2AF). The zero crossing technique, MOA4, was utilized to determine the atrial flutter MOAs (AFMOAs).

A simple root mean square (rms) method for analyzing the SNR for each of the data channels was employed with Equ. 4 and 5. The SNR was also measured over the intervals, as will be described, and referred to as interval-SNR.

$$S_{rms} = \sqrt{\frac{1}{N} \sum_{n=1}^{N} \left(\frac{1}{M} \sum_{m=1}^{M} S_{mn} \right)^2} \qquad\qquad \text{Eq. 4}$$

$$N_{rms} = \sqrt{\frac{1}{N} \sum_{n=1}^{N} \frac{1}{M-1} \sum_{m=1}^{M} \left(S_{mn} - \mu_n \right)^2} \qquad\qquad \text{Eq. 5}$$

where N, the number of samples in the window, was 800. M indicates the number of windows or QRS complexes found, S_{mn} is the data sample at point (m,n) and μ_n is the mean of the time-aligned samples at location n of the windows. S_{rms} is the rms value of the signal and N_{rms} is the rms value of the noise. For the interval-SNR, S_{rms} was measured over the QRS complex and N_{rms} was measured over the PQ interval. Another method used for establishing the SNR was similar to that used by Wu et al. [14]. Since our data was acquired directly, rather than by computation from the potential differences among several adjacent disc sensors, the noise ratios had to be slightly modified by removing the double summation. We also changed the interval over which the noise level was determined from the PR interval to the PQ interval. In classical signal theory,

SNR is generally known as the rms SNR, which is the ratio of the square root of the signal power to the square root of the noise power. In this research we are using the ratio of S_{rms} to N_{rms}.

Our ultimate goal is to display the activation map on the dynamic virtual image of the beating heart. As a first step, to project the MOA maps on the simulated human torso, a cylinder with a radius of 1cm and 20 sequential circumferential segments was utilized. The subject's chest circumference was measured at the time of recording. The first approximation model to the true chest surface assumes it to be a cylinder in which the surface of another simple solid, such as a sphere offset from the axis of the chest represents the range where depolarization wavefronts occur. The transformation obviously introduces some distortion as it preserves the distances of each sensor from the two axes on the chest (the midsternal line and the line connecting the nipples). A vertical line of symmetry is included, corresponding to the manubrium and xiphoid process. The circumference was measured at the horizontal reference line crossing the nipples. For some women this introduced potential errors. The contour map was then transposed onto the surface of the cylinder in its proper location. These maps can be viewed in a 3D perspective on the computer monitor and rotated for different views.

3 Results

Fig. 3 shows the recording sites on the torso of each normal subject. **Figure 3 about here.**

Fig. 4 illustrates a BSMOAM of a normal subject, WF. The legend for this, and all other BSMOAMs to follow, will depict the MOAs preceding the L2R lighter and negative, while MOAs following the L2R are darker, positive. The MOA times for the contour lines are labeled for each of these types of figures. The range of MOAs for Fig. 4 is –26 to 49ms

with respect to L2R. There are two areas, depicting earlier depolarizations, separated by a delayed region. The earliest activation, not in the map, occurred approximately 30ms prior to the L2R. Fig. 5 shows the 24 recording sites for subject AS, four other sites were rejected for having too low SNRs. Fig. 6 shows a BSMOAM from the accepted recording sites, based on the local SNR, of subject AS. The negative times are prior to the L2R. Figure 7 shows contours for atrial flutter subject AS transposed onto the cylinder model. The bold circle depicts the nipple line; the vertical bold line is the Y-axis. Closely spaced contour lines signify slower moving wavefronts, as in the upper right corner of the map (x=0.5, y=0.1). This is the area of earliest activation: MOA = -6.4ms, from where the wavefront originates and slowly radiates outward. In all other areas of Fig. 7 the activation wavefronts move faster, hence there are fewer contours. The white background should not be misconstrued as areas of early activation.

Figure 4 about here

Figure 5 about here

Figure 6 about here

Figure 7 about here

Figure 8 also illustrates subject AS. The AFMOAs were contoured to produce this body surface map. The rate of propagation of the activation is shown with a quiver plot. The larger arrows signify more rapid propagation.

Figure 8 about here

A single factor analysis of variance (ANOVA), in reference to the MOAs, was performed at a significance level of 1% for the normal subjects to test the null hypothesis

that all the MOAs have been drawn from the same parent population. The F critical value was found to be 3.227. The F statistic from the ANOVA was 1.769 with a P value of 0.127, therefore the hypothesis is not rejected that these MOAs were from the same population. A comparison of the pathological MOAs could not be done as those were recorded from a less than uniform array of locations.

The Wiener-filtered interval SNR for the normal subjects was 7.4 ± 4.91 ($\mu \pm \sigma$), while the raw SNR was 5.24 ± 4.1 ($\mu \pm \sigma$). This resulted in a SNR gain of 3 dB. The N/S_{rms}, as defined by Wu et al. [14], the noise level to the averaged rms values of signals over the chest during the QRS complex for these subjects was 6.6% ± 6.0 %. For the pathological subjects the Wiener filtered interval SNR was 4.53 ± 2.18 ($\mu \pm \sigma$) with the raw SNR 3.64 ± 1.87 ($\mu \pm \sigma$) resulting in a SNR gain of 1.9 dB. The N/S_{rms} was 23.0% ± 12.0 %.

4 Discussion and Conclusions

This article is intended to be a work-in-progress report. The number of subjects studied in this paper is too limited for firm conclusions regarding the diagnostic capabilities of the MOAMs. However, the techniques for processing the LECG data and generating BSMOAMs are clearly in place. We have found an adequate method to determine the MOAs, but feel that the process may be improved considerably.

Figure 3 shows that the recording sites for the normal subjects were uniform. In contrast, Fig. 5 shows that the recording sites for the atrial flutter subject were not uniform, and this was typical for all the pathological recordings. Direct comparisons between normal subjects and pathological subjects have not been done. Comparisons between pathological subjects are also difficult, due to the non-uniformity of recording sites.

Figure 4 is a BSMOA map from normal subject WF. There are two areas of early activation, typical of all six normal subjects in the upper right corner and left bottom corner of the maps. These were not in the exact same locations for each of the normals, but we did neither correct for, nor consider morphological differences. The validation and diagnostic interpretation of these maps will only be possible with concurrent intracardiac and Laplacian recordings. We do have plans to perform such studies in the future.

Figure 6 displays a BSMOAM for the atrial flutter subject AS. It should be noted that the earliest (lightest) area in this map is in the upper center, approximately –6.4ms. This is actually a similar location to one of the early activation areas for the normal subjects. The second early activation sight for the normals is not seen in the atrial flutter case. As the recording sites were different from those on the normal subjects, these can not be compared directly. Whether the absence of this second early activation region is characteristic of atrial flutter is yet to be determined.

For illustration of the method, Fig. 7 shows the cylinder model of the torso with a MOAM imposed for atrial flutter subject AS. Any map may be presented in this manner. This model is still under development and will be enhanced in the future: initially to present a more accurate model of the torso, and later, the heart's surface. Ultimately, we expect the MOAM to be projected on the beating image of the heart. This cylinder as well as the improved models to be developed, can be interactively manipulated on the video screen to allow the viewing of any area of interest that may be out of sight, but accessible. We have not established whether the back of the torso may be included in recordings. We may zoom in and out to view details, mark specific areas of interest, and save the image for future reference. Naturally, more recording sites over a larger torso area are necessary to take full advantage of the rotatable display.

Figure 8 shows part of an atrial flutter cycle from the same subject, AS. This is a different way of depicting the activation sequence. Fig. 6 showed activation with respect

to L2R, while this figure shows activation with respect to the peaks of surface flutter waves. The number of contours on this map was minimized to emphasize the quiver plot. The arrows illustrate two areas where activation spreads quickly during atrial flutter. One of these areas is around (x=5, y=2) where the contour originates at approximately 60ms prior to the L2 atrial flutter (L2AF). The (x=12, y=-8) neighborhood is activated about 40ms prior to the L2AF. We expect that these recordings will be realized with sufficient spatial resolution to map a complete flutter cycle to show the point of re-entry.

The SNRs were generally higher for the normals than for the pathological subjects. This may partly be due to the difference in the sites recorded in the two groups, but the normal subjects were all younger, with considerably less body fat, although we did not quantify this parameter. The sites for the normals were uniform and frontal. Some of the pathological recordings were from the axillary zone and even from the back.

Based on the Wiener filtered data analyzed over the heart cycle, the SNR improved by 3.0 dB for the normals and 1.9 dB for the pathological subjects. The noise level in our recordings was far greater than that reported by Wu et al. [14] and He and Wu [15], but they took far more precautions to minimize the noise, such as skin preparation, and recorded in an electrically shielded room, while our pathological data was collected in ordinary hospital rooms and under considerable time pressure. The normals were recorded in an ordinary electronics laboratory, and without any skin preparation. The Wiener filter utilized for this research is not the same one reported by He [16].

In conclusion, BSMOAM production techniques have been presented and illustrated for normal subjects and a pathological case of atrial flutter. A partial atrial flutter cycle map was generated with a quiver plot to show the fast and slow moving activation areas. More locations need to be recorded to achieve finer resolution of the progress of activation. This technique should be useful in viewing complete cycles to

determine re-entry points. The method may also be useful for displaying areas of different conduction rates around acute and chronic infarcts.

Whether these patterns are characteristic for those subjects with similar arrhythmias, still needs to be determined. That task is beyond the scope of this report. We plan to process and analyze more subjects with specific arrhythmias, using similar techniques to those presented here. Our existing and future database should be useful to establish whether specific patterns identify certain pathologies. Lu already identified differences between small groups of subjects with bundle branch blocks [20]. The LECG for LBBB and RBBB subjects showed distinct characteristics.

5 References

1. L Nahum, A Mauro, H Chernoff, and R Sikand, "Instantaneous Equipotential Distribution on Surface of the Human Body for Various Instants in the Cardiac Cycle." *Appl. Physiol*. 3, pp. 454-464, 1951.

2. B Taccardi and G Marchetti, "Distribution of Heart Potentials on the Body Surface and in Artificial Conducting Media," *The Instituto Di Cardiologia Sperimentale Dei Servizi Scientifici Simes.* Milan, Italy, 1963.

3. R Karsh, M Spach, and R Barr, "Interpretation of Isopotential Surface Maps in Patients with Ostium Primum and Secundum Atrial Defects," *Circulation*. 41(6), pp. 913-933, 1970.

Electromagnetics, vol. 21, pp. 621-632, 2001.

4. M Spach, RC Barr, NC Durham, "The Use of Isopotential Surface Maps in Understanding Clinical ECGs," *Amer. J Dis Child*; 124(9), pp. 359-363, 1972.

5. D Mirvis, "Body Surface Distribution of Electrical Potential During Atrial Depolarization and Repolarization," *Circulation*. 62(1), pp. 167-173, 1980.

6. W Smith, and R Ideker, "Computer Techniques for Epicardial and Endocardial Mapping," *Progress in Cardiovascular Diseases*. 26, pp. 15-32, July/August 1983.

7. V Fattorusso and J Tilmant, "Exploration du champ electrique precordial a l'aide de deux electrodes circulaires, concentriques et rapprochees," *Arch. Mal du Coeur*. 42, pp. 452-455, 1949.

8. A Van Oosterom, and J Strackee, "Computing the Lead Field of Electrodes with Axial Symmetry," *Medical & Biological Engineering & Computing*. (21), pp. 473-481, 1983.

9. M Kaufer, "Optimization of Concentric Tripolar Ring Sensors," *MS BME Thesis*, University of Miami, 1992.

10. D Geselowitz, and J Ferrara, "Is Accurate Recording of the ECG Surface Laplacian Feasible?" *IEEE Trans. BME*. 46(4), pp. 377-381, 1999.

11. B Hjorth, "An On-Line Transformation of EEG Scalp Potentials into Orthogonal Source Derivations," *EEG and Clin. Neurophysiology*, 39, pp. 526-530, 1975.

12. B He, and RJ Cohen, "Body Surface Laplacian ECG Mapping," *IEEE Trans. on BME*. 39(11), pp. 1179-1191, 1992.

13. B He, and RJ Cohen, "Body Surface Laplacian Mapping in Man," *IEEE EMBS* 13(2), pp. 784-786, 1991.

14. D Wu, HC Tsai and B He, "On the Estimation of the Laplacian Electrocardiogram during Ventricular Activation," *Ann. BME,* August 1999.

15. B He and D Wu, "Laplacian Electrocardiography," *Crit. Rev. BME*, vol.27 (3-5), pp.285-338, 1999.

Electromagnetics, vol. 21, pp. 621-632, 2001.

16. B He, "Theory and Applications of Body-Surface Laplacian ECG Mapping," *IEEE Eng. Med. Biol., vol.17, pp.102-109, 1998.*

17. CC Lu, PP Tarjan, "An Ultra-High Common Mode Rejection Ratio (CMRR) AC Instrumentation Amplifier for Laplacian Electrocardiographic Measurements," *Biomed. Instr. & Tech*. pp. 76-93, Jan.-Feb, 1999.

18. CC Lu, R Plourde, WF Fang, S Uhlhorn and PP Tarjan, "Laplacian Electrocardiograms with Active Electrodes for Arrhythmia Detection," IEEE EMBS Proc. Ann. Conf. Chicago, IL, 10/95.

19. CC Lu, R Plourde, WF Fang, S Uhlhorn and PP Tarjan, "Laplacian Electrocardiograms with Active Electrodes," IEEE Proc. Southern BMES Ann. Conf. Biloxi, MS, 4/97.

20. CC Lu, "Non Invasive Laplacian Detection Using Active Concentric Ring Sensors*."* *Ph.D. Dissertation*, University of Miami, June 1998.

21. O Bertrand, L Garcia-Larrea, F Artru, F Mauguiere and J Pernier, " Brain-stem Monitoring I. A System for High-rate Sequential BAEP Recording and Feature Extraction," *EEG and Clin. Neurophysiology*, 68, pp. 433-445, 1987.
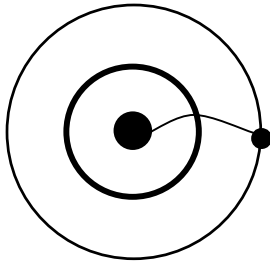
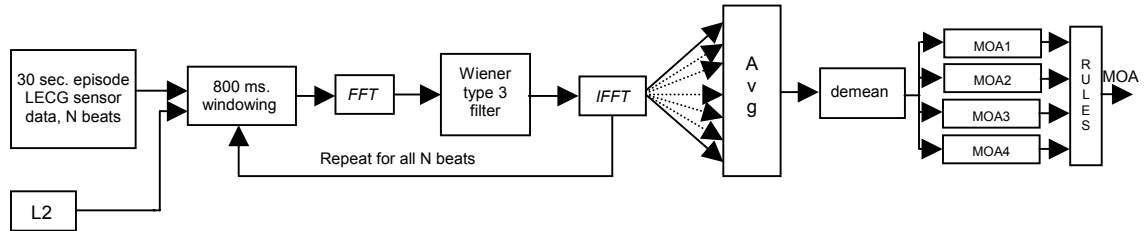**Figure 1. The electrode configuration of the active sensor.**

Figure 2. Data processing for one LECG active sensor for MOA determination.
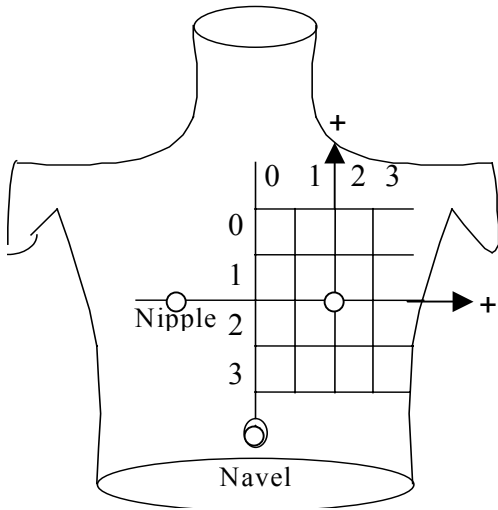

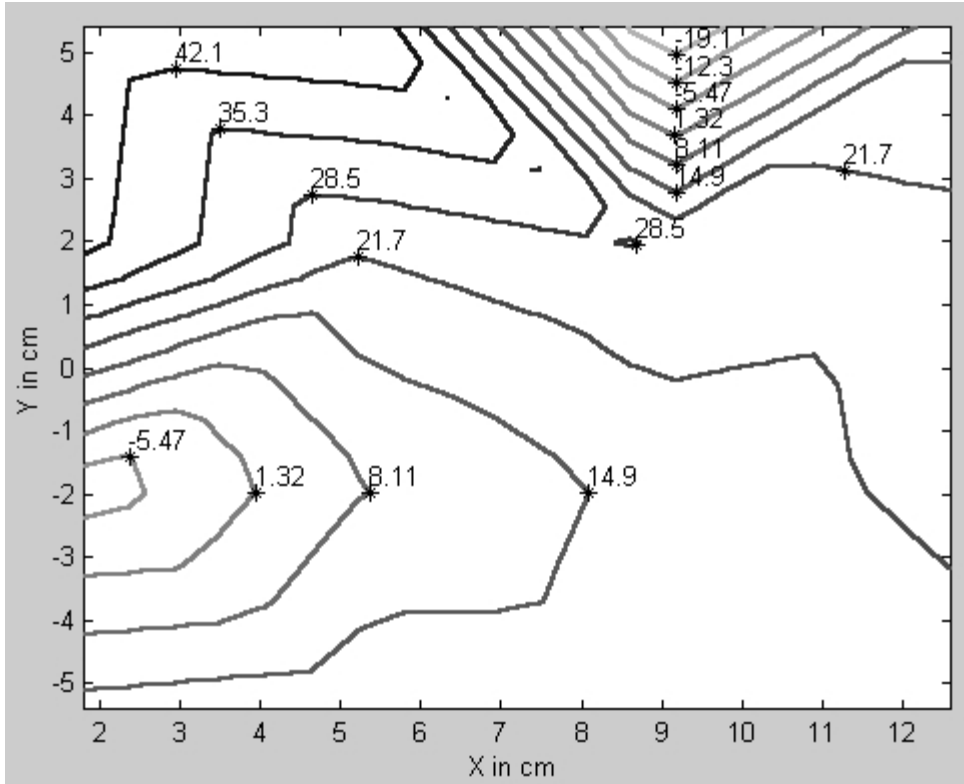**Figure 3. The 4x4 grid depicting recording sites of normal subjects.**

Figure 4. BSMOAM of normal subject WF displaying two early activation areas. The earliest activation is in the top right of the figure and is approximately 30ms prior to the L2R but does not show up with this low-resolution contour. The other is in the left middle with an early activation of approximately 10ms prior to the L2R. These two early areas were common in the normal subjects. The latest area is approximately 49ms after the L2R in the upper left corner.
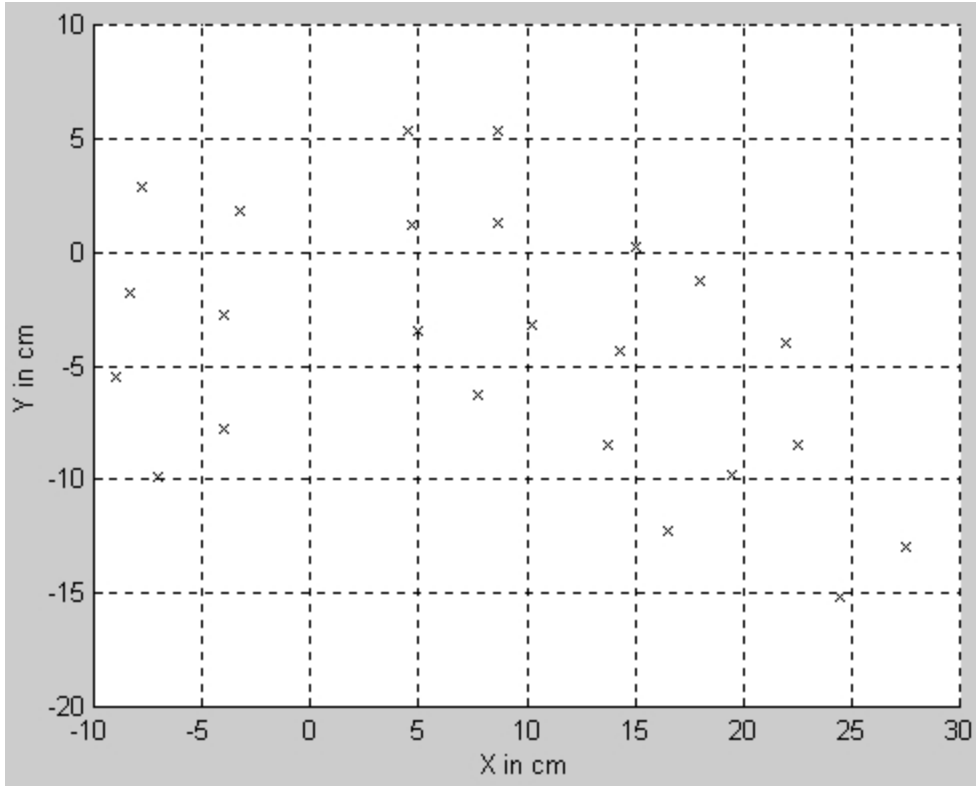
Figure 5. The recording sites of atrial flutter subject AS that were accepted for mapping.
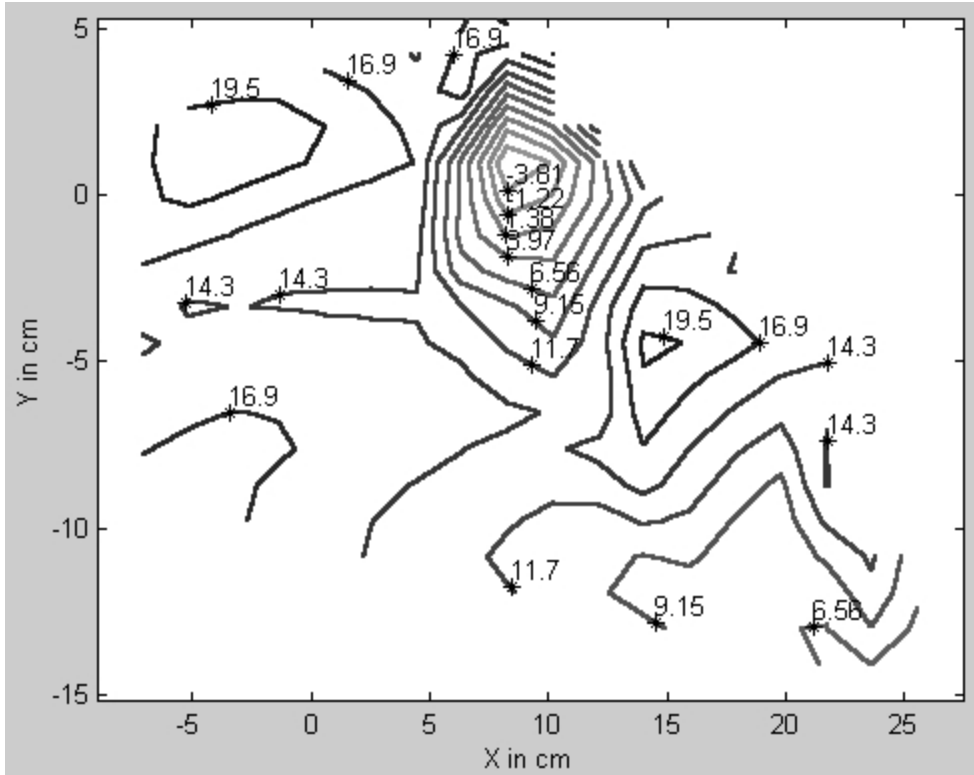
Figure 6. BSMOAM of atrial flutter subject AS. The top center has an early area similar to the normal subjects. The early areas are activated prior to the L2R. The earliest activation was 6.4ms prior to the L2R and the latest activation was approximately 22ms after the L2R. At this resolution of contouring the extreme limits are not included.
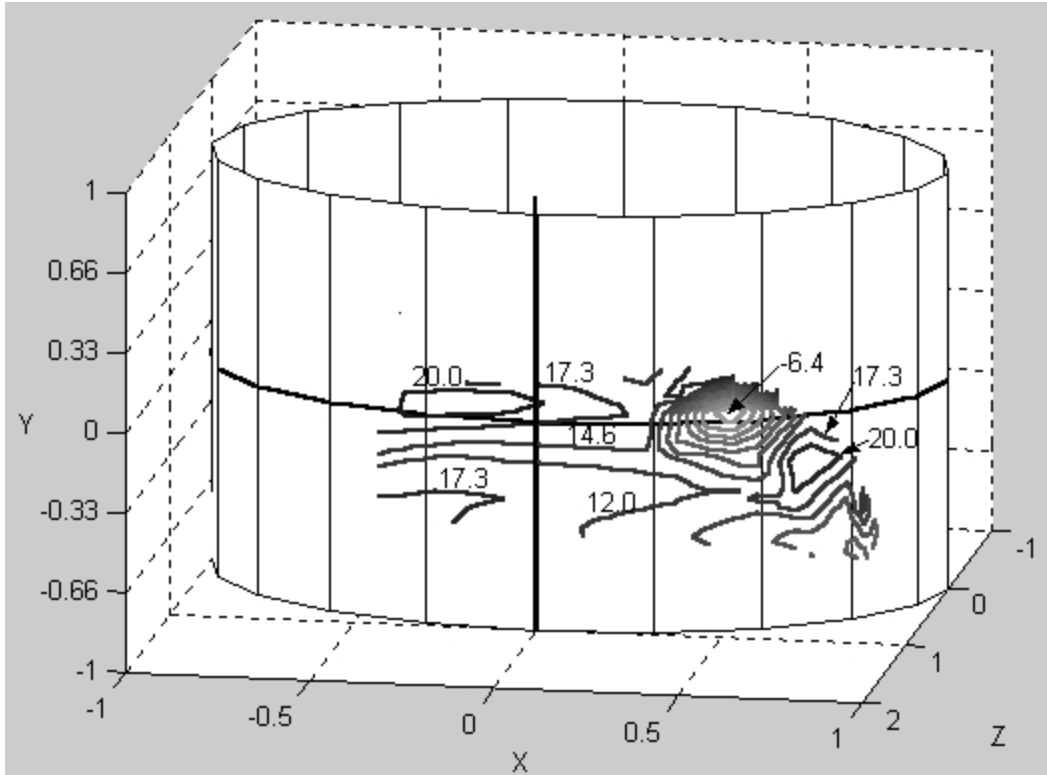
Figure 7. Cylinder model of torso with BSMOAM of atrial flutter subject AS transposed onto the surface. The bold circle depicts the nipple line; the vertical bold line is the Y-axis. Closely spaced contour lines signify slower moving wavefronts, as in the upper right corner of the map (x=0.5, y=0.1). This is the area of earliest activation: MOA = -6.4ms, from where the wavefront originates and slowly radiates outward. In all other areas of Fig. 7 the activation wavefronts move faster, hence there are fewer contours. The white background should not be misconstrued as areas of early activation.
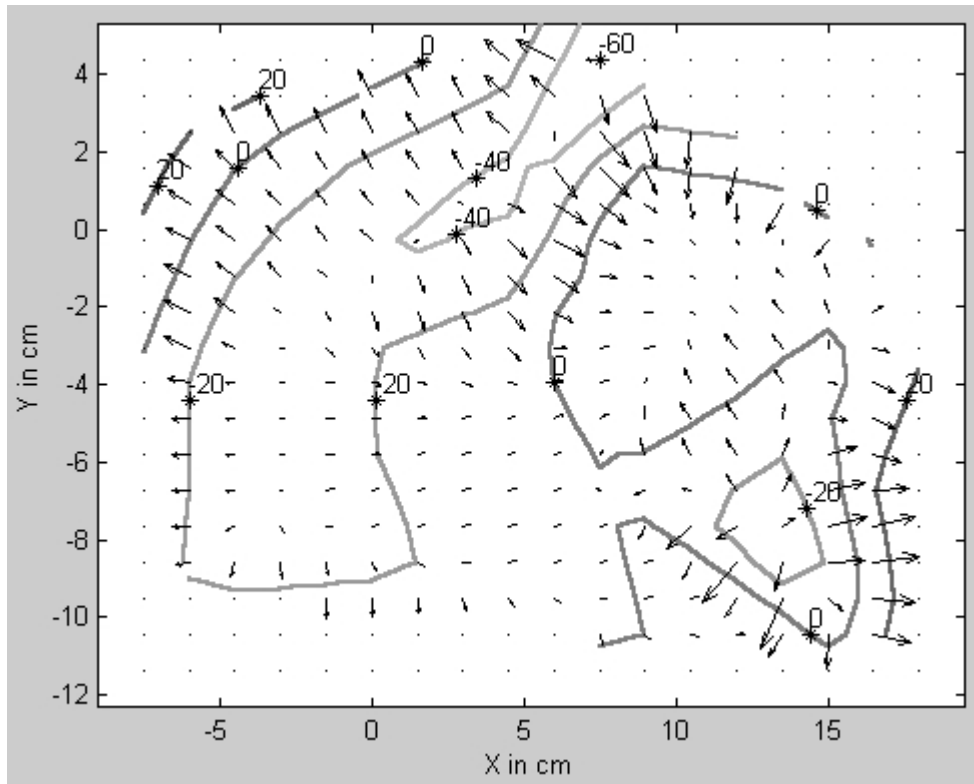
Figure 8. Body surface contours of the active atrial flutter locations recorded from subject AS. The rate of propagation of the atrial flutter activation is shown with a quiver plot. The larger arrows signify more rapid propagation. This shows two major areas where the activity appears to be originating, top center and lower right. The top center area is 60ms prior to the L2AF and the lower right area is approximately 40ms prior to the L2AF.